

A Multi-Resolution watershed-based approach for the segmentation of Diffusion Tensor Images

P.R. Rodrigues¹, A. Jalba², P. Fillard³, A. Vilanova¹, and B.M. ter Haar Romeny¹

¹ Department of Biomedical Engineering, Eindhoven University of Technology, WH 2.111, 5600 MB Eindhoven, The Netherlands

P.R.Rodrigues@tue.nl

² Department of Computer Science, Eindhoven University of Technology, 5600 MB Eindhoven, The Netherlands

³ NeuroSpin, Saclay, France

Abstract. The analysis and visualisation of Diffusion Tensor Images (DTI) is still a challenge since it is multi-valued and exploratory in nature: tensors, fiber tracts, bundles. This quickly leads to clutter problems in visualisation but also in analysis.

In this paper, a new framework for the multi-resolution analysis of DTI is proposed. Based on fast and greedy watersheds operating on a multi-scale representation of a DTI image, a hierarchical depiction of a DTI image is determined conveying a global-to-local view of the fibrous structure of the analysed tissue. The multi-resolution watershed transform provides a coarse to fine partitioning of the data based on the (in)homogeneity of the gradient field. With a transversal cross scale linking of the basins (regions), a hierarchical representation is established.

This framework besides providing a novel hierarchical way to analyse DTI data, allows a simple and interactive segmentation tool where different bundles can be segmented at different resolutions.

We present preliminary experimental results supporting the validity of the proposed method.

1 Introduction

In the fairly recent Diffusion Weighted MRI acquisition techniques, introduced by Basser [1], Diffusion Tensor Imaging (DTI) is subject of intense research due to its feasibility in clinical practice, simplicity and established mathematical frameworks. DTI constitutes a valuable tool to inspect fibrous structures in a non-invasive way. Among the most important applications of DTI is the study of brain connectivity or fibrous structure of muscle tissues such as the heart [2, 3]. DTI has also been used to identify abnormalities in several diseases such as stroke, schizophrenia and multiple sclerosis [4].

In DTI, at least six gradient directions are measured, enough to compute the *diffusion tensor* (DT) per voxel, representing the local pattern of directional tissue diffusivity. Formally, a diffusion tensor is a 3×3 positive definite symmetric matrix.

A common way to visualize the tensor data (Vilanova et al. [2]) is by fiber tracking. Given the DT field, fiber tracking techniques try to reconstruct the

fibrous structures (i.e., fiber tracts). In several applications higher semantic level structures, e.g., coherent white matter bundles such as the *corpus callosum* or the *corticospinal tract*, are of greater interest [5–8]. This hierarchical nature of the information, i.e., tensors, fiber tracts, bundles, pathologies, drives the inspection of this data to be exploratory in essence.

Clustering techniques have been used to group individual fiber tracts into coherent structures [9]. However these methods deal with derived structures from the tensor field (i.e., do not use directly the full tensor information), therefore they are very sensitive to the used fiber tracking method. An alternative to clustering fibers is the direct segmentation of the tensor field in volumetric regions.

Image segmentation is necessary to determine regions of interest where subsequent quantitative analysis and visualisation is performed. It provides tools to extract shape, appearance and other structural features than can then be used for the analysis of pathologies, or, for instance, to identify the cognitive development of different types of population such as neonates or elderly people.

Scalar image segmentation has been widely studied and different algorithms have been proposed through the years. However, the relatively new DTI segmentation is still a challenging task. Some approaches have been proposed [5–7, 10] though, they often do not allow a full segmentation of the data, i.e., they segment one object at a time, have a multitude of parameters that must be set to achieve the desired result and have limited user interaction, preventing the added value of clinical users’ expert knowledge in the segmentation.

In this work, we use a multi-scale watershed algorithm for the segmentation of DTI structures. The driving idea behind our framework is to help the user *focus* on accomplishing a given *analysis task*, by first presenting a *simplified* view of the data, while still maintaining a global one (i.e. *context*). While *segmentation* is an obvious usage, our framework allows for more general tasks. For example, the ability to focus on a given ROI may help in exploratory analysis and statistical studies, as the user is presented a greatly simplified view of the data.

Given an input DTI, a *scale-space* representation is constructed [11]. The main motivation is that when increasing the scale, small details due to noise disappear, while main fibrous tissue structures (having predominant orientations) can still be reliably recovered. At each scale a watershed transform [12] is applied. Ideally, a structure would be outlined by a single region, however, in many situations, specially given the anisotropic nature of the involved tissues, the watersheds do not directly resolve to the anatomical structures. By linking several regions across scales, we infer a meaningful hierarchical representation of the data allowing novel ways to analyse and visualise diffusion tensor fields.

The main contributions of this paper are:

- a *hierarchical representation* of the diffusion tensor field, which allows for *interactive grouping*, in an exploratory manner;
- a method for *linking* several interest regions across *scales*, such that one can infer a meaningful hierarchical representation of the data, unravelling novel ways to study diffusion tensor fields;
- a *multi-resolution segmentation* method, presented as a proof of concept of the proposed framework.

The multi-resolution watershed segmentation method is presented in Section 3. In Section 4 experimental results are presented supporting the validity of the methods.

2 Background

Different algorithms have been proposed for the segmentation of tensor fields. Zhukov et al [6] proposed a level-set method over a scalar field derived from anisotropy measures. However this method fails to distinguish between regions with same anisotropy but different direction.

Level-set methods using the full tensor information have been proposed by Zhizhou and Vemuri [5] and Rousson et al [7], however, these iterative gradient descent based solutions seek a local solution and therefore are highly sensitive to initialization and parameter settings.

Watershed based methods, such as proposed by Rittner and Lotufo [12], are well known by their over segmentation results. More recent and more efficient methods like the globally optimal graph-cuts have been applied to DTI by Welde-selassie and Hanarneh [10], however they provide a binary partition of the data, into one object and the background.

More recent work, such as Niethammer et al. [13], focus on the specific problem of segmenting a tubular structure such as the *cingulum*.

The concept of scale space has been widely studied in the image analysis field [14, 15]. An image is represented as a one-parameter family of blurred images. It derives from the observation that objects are composed of different structures at different scales and therefore may appear different at different scales. The attractiveness of the method lies also in the link between scale-space theory and the biological process of vision.

Scale-space theory has been widely explored in many medical imaging problems. In Dam's work [16] for the multi-scale segmentation of scalar volumes, such as Computed tomography (CT) images, a volume is partitioned in several regions and it's up to the user to sculpt his desired object by selecting the appropriate 'building blocks' in different scales. Although a somewhat cumbersome practice, given the gain in speed by orders of magnitude, compared to manual segmentation, this work has been used in clinical setup with promising results.

Following the definition of a consistent multi-scale space for semi positive definite tensors by Florack and Astola [11] we extend such multi-resolution geometric studies to diffusion tensors fields. We present a multi-resolution segmentation algorithm that operates by applying the watershed transform to the different images in a generated DTI scale-space. The well-known watershed's over-segmentation, a shortcoming in most cases, is actually a core element of the presented framework.

This fast and simple partitioning of the image, applied to each level in the scale-space, allows the creation of the hierarchical representation of the data. This establishes an automated, general and interactive segmentation framework that equips the user with tools to explore and quickly segment the data.

3 Multi-Resolution Watershed Segmentation

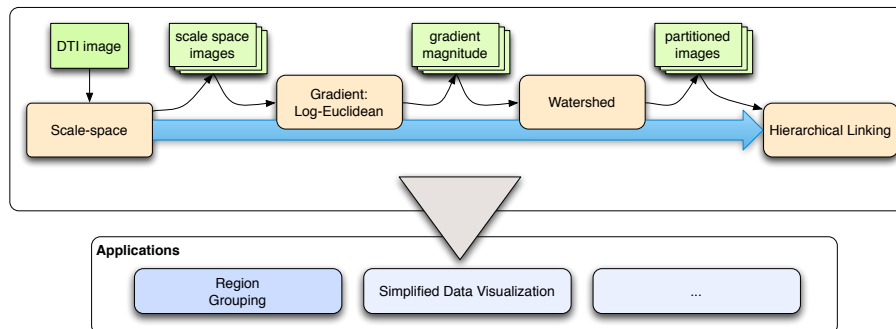


Fig. 1. Global gist of the hierarchical segmentation.

In the following, we describe the several stages involved in the creation of a hierarchical representation of the data, see Figure 1 for a global gist of the process. A scale space stack of tensor field images is created by successively blurring the acquired DTI image. To each of these images, the watershed transform is applied, thus obtaining a partitioning of the structures at each scale. Next, the several basins are linked to each other in a bottom-to-top manner. With this pipeline a hierarchical representation of the data is obtained allowing further visualization/interaction possibilities.

3.1 Scale-Space Representation of DTI

Florack and Astola [11] formulated a consistent scale-space representation for symmetric positive definite tensors. This follows the work proposed by Arsigny et al., Pennec et al., and Fillard et al. [17–19], e.g. the so-called log-Euclidean framework. The multi-scale representation for a tensor field f , at scale σ is achieved by the blurring operator

$$F(f, \sigma) = \text{Exp}(\text{Log } f * \phi_\sigma), \quad (1)$$

where $\text{Exp}(\cdot)$ is the exponential map, $\text{Log}(\cdot)$ is its unique inverse, i.e. the logarithmic map, and ϕ_σ is the isotropic Gaussian scale-space kernel in n dimensions, i.e.,

$$\phi_\sigma(x) = \frac{1}{\sqrt{2\pi\sigma^2}^n} \exp\left(-\frac{1}{2} \frac{\|x\|^2}{\sigma^2}\right). \quad (2)$$

Since in a multi-scale representation all scales are equivalent, a natural way to probe the archetype of DTI data is provided, resulting in a **coarse-to-fine** approach, see Figure 2.

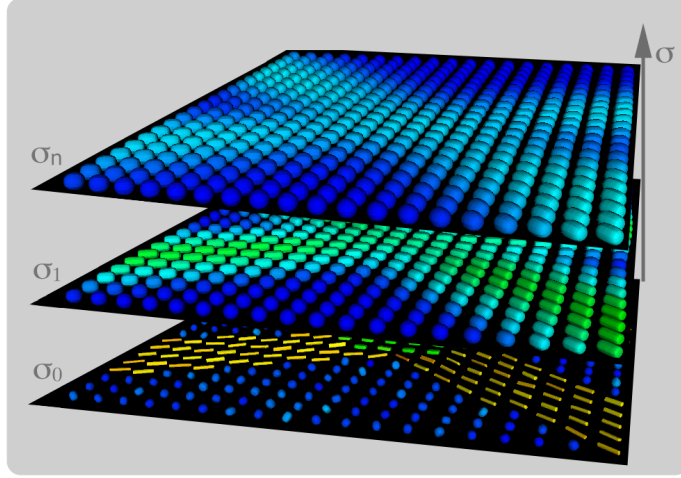


Fig. 2. Superquadratic glyphs [20] illustrating Eq. (1) for five exponentially increasing scales σ_i . The synthetic DTI shows two fiber bundles crossing at a 65° angle.

3.2 Watershed Representation

The *watershed method* regards an image as a topological map, a landscape. As rain falls, water gathers in pools from the lowest points in the landscape. The landscape defines these pools, the *catchment basins*. As the water level rises, dams are built to prevent the merging of the pools. These boundaries constitute the *watersheds*. This concept was introduced by mathematicians in [21]. The watershed provides a simple partitioning of the image based not on the original one but on a dissimilarity image. The gradient magnitude is a typical, simple and general measure defining region borders from the image edges.

At each scale, the Log-Euclidean gradient [17]

$$d_{LE}(\mathbf{A}, \mathbf{B}) = \sqrt{\text{tr}((\text{Log}(\mathbf{A}) - \text{Log}(\mathbf{B}))^2)} \quad (3)$$

is applied, hence objects are outlined with respect to the scale at which the gradient is calculated. Naturally, different object sizes require different scales.

Other dissimilarity measures for DTI watershed segmentation have been proposed such as in Rittner and Lotufo [22]. However, many different distance measures have been proposed (Peeters and Rodrigues et al [23] for a survey), but they capture different DT degrees of freedom, thus which one to use is a problem *per se*. For consistency with the scale-space representation of the DTI data, we used the Log-Euclidean gradient as a common and generic dissimilarity measure.

3.3 Cross-Scale Linking

Well-known scale-space theory [14] studies the progression of basins across scales. Because, each basin is intrinsically related to the local minimum of the gradient magnitude, succinctly, basins can be afflicted by annihilation, creation, merge and split events. As the scale increases, the number of catchment basins decrease

- they gradually merge into larger basins. These minima can be tracked by a linking process, forming a singularity string, across scales. With this process, we combine the simplification provided by the (high level) selection scale with the fine scale basins in the (low level) representation scale (see Figure 3). This method has been implemented for clinical use in medical imaging with promising results [16].

Conceptually, in an iterative process, a region in a given scale is linked to the region at the next scale with maximum spatial overlap. From this linking process, a hierarchical representation of the data results, where each basin is linked to exactly one region at the next higher scale level, see also Figure 5. This linking tree can be used for a "region focusing" process, where a simplified region at a selection scale is substituted by the regions at the lower representation scale. This selection scale determines the abstraction level that the user chooses to inspect the data, i.e., how simplified the data is.

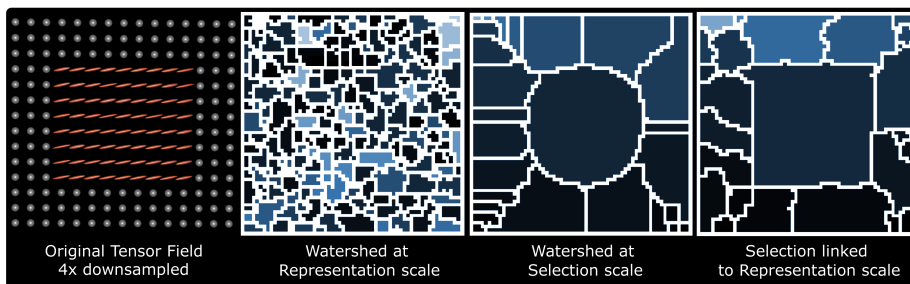


Fig. 3. Region focusing across scales. Following the linking tree from the selection scale to the representation scale, fine detail is obtained; last image shows the regions at the *Selection scale* represented with basins of the lower, *Representation scale*.

The stack of scale-space images is produced by blurring the data-scale DTI image with increasing σ . In order to obtain a sufficiently fine space, considering its exponential nature, σ is changed per scale i

$$\sigma_i = \sigma_0 \exp(\lambda_i) , \lambda_i = i \frac{-\ln(\Delta_\lambda)}{3} , \quad (4)$$

where parameter Δ_λ indicates the ratio at which the number of basins decrease, see Figure 4.

3.4 Region Grouping

With a partitioned *Selection Scale*, given by applying the watershed transform to the selected scale, a connectivity graph $G(n_i, e_j)$ is built where: each node n_i holds the Log-Euclidean mean tensor [17], representing the corresponding basin; each edge e_j holds the Log-Euclidean distance [17] between each neighbouring basin. The average weight of all the edges within users' selected basins (sample seeding basins) μ is taken as predicate to a simple region growing algorithm

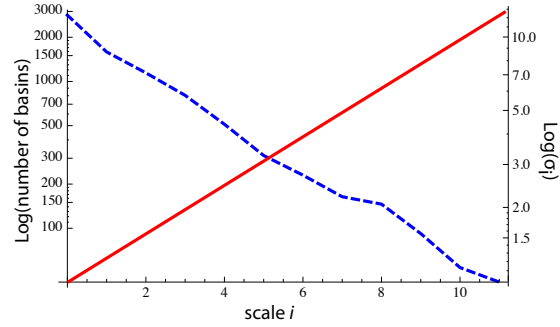


Fig. 4. Graph plot showing the relation between increasing the scale-space parameter σ and the (decreasing) number of basins, using $\Delta_\lambda = 0.5$.

operating on the edges in graph G . A new, spatially connected, basin is added if the edge connecting it to the growing region is less than the average $\mu \times r$, where r is a user define ratio. This algorithm, quickly groups similar connected basins. These can then be 'focussed' to the lowest Representation Scale.

4 Results

The synthetic image shown in Figure 5 has five distinct regions, with different DT populations. Despite having distinct DTs, some properties are shared between regions but are different to others, e.g., R4 has the same anisotropy as R3 and R5, but different main diffusivity direction to R3. With this synthetic data we illustrate the hierarchical nature of the proposed segmentation.

The DT in the five regions have realistic eigenvalues: $\lambda_{R1} = [3, 10, 10] \times 10^{-3} mm^2/s$, $\lambda_{R2} = [5, 5, 5] \times 10^{-3} mm^2/s$, $\lambda_{R3} = [14, 2, 2] \times 10^{-3} mm^2/s$, $\lambda_{R4} = [17, 3, 3] \times 10^{-3} mm^2/s$ and $\lambda_{R5} = [17, 3, 3] \times 10^{-3} mm^2/s$. In order to mimic a real DTI acquisition, noise was added to the 128×128 synthetic image. From the noiseless DTs, using the inverse Stejskal Tanner [24] relation, the signal attenuations were obtained. To each direction value, Rician noise was added with $SNR = 15.3$, and the tensors re-estimated.

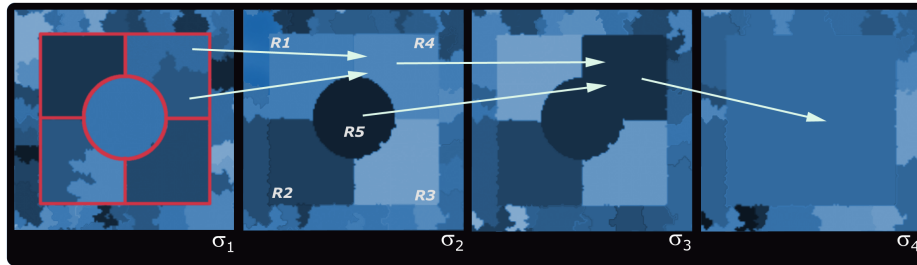


Fig. 5. The hierarchical nature of the watershed scale-space segmentation. Different basins are linked to the ones above. Colours indicate different regions. Red outline indicates the original five regions.

Figure 5 shows the obtained basins for the computed scale space. We can see the segmentation consequences of choosing appropriate selection scales and

automatically tracking down objects to the lowest representation scale. As the selection scale decreases, we clearly see the hierarchical segmentation occurring. At Scale σ_3 we obtain regions R4 and R5 as a unique object, since they are very similar, whereas at scale σ_2 , these two regions constitute different segmentation objects.

Figure 6 shows the results of the semi-automatic segmentation tool provided by the method. In a $30 \times 30 \times 20$ volume, two fiber bundles forming 'tubes' with radii of 2 voxels intersect each other. Here, the tensors, with eigenvalues $\lambda = [17, 3, 3] \times 10^{-3} mm^2/s$ and oriented tangentially to the centre line of the tube, are estimated using a mixed tensor model, as in [25]. Rician noise is added with $SNR = 15.3$. In this experiment, due to the use of an isotropic Gaussian scale-space kernel, no appropriate selection scale is found in order to achieve the desired segmentation: automatically distinguish the two tubes. Users' knowledge is here utilized. An appropriate Selection scale is chosen by the user, i.e., an appropriate simplification of the data is selected. Then, in a typical visualisation such as FA map, the user interactively picks some points in the structure of interest (see Figure 6). These points select the correspondent basins, at the simplified Selection scale, which are then linked down to the Representation scale aggregating the several voxels forming the final segmentation.

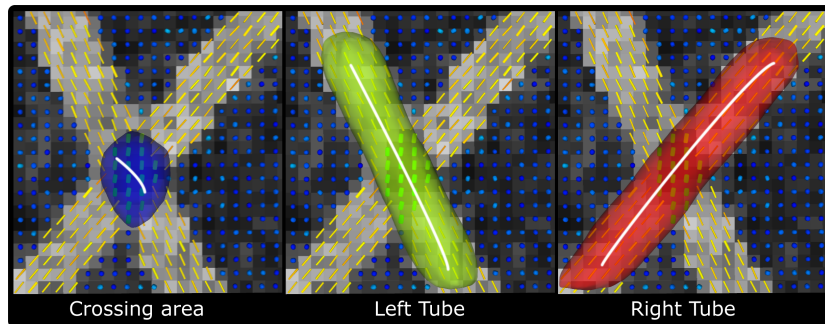


Fig. 6. Synthetic image with two crossing tubes. User's interactive picking are represented by the white lines. Three segmentation results arise depending on the stroke selection: crossing region, tube one or tube two.

Employing an isotropic Gaussian kernel, in a real brain dataset, as in Figure 7, fails to deliver an appropriate high level selection scale for the automatic segmentation of the larger structures. Brain tissue, white matter, manifests itself in DTI images as anisotropic structures. In the isotropic scale space, these structures of interest successively disappear. Nevertheless, the semi automatic segmentation still gives satisfactory results.

A typical user interaction follows, as illustrated in Figure 7:

1. An appropriate Selection scale is chosen, by inspection of the level of simplification provided by a scale, with a view of the correspondent basins;

2. In a typical main eigenvector RGB colour mapping (Figure 7(left)), by stroking some points in the image, seeding basins at the chosen scale are selected (Figure 7(middle));
3. The region grouping algorithm collects similar connected basins, which are then 'focussed' into the Representation scale.

Figure 7(right) shows two bundles segmented in two different scales: the *corpus callosum* in red, visible in a higher scale σ_4 ; and the *cingulum* in green, visible in a lower, more detail scale σ_4 .

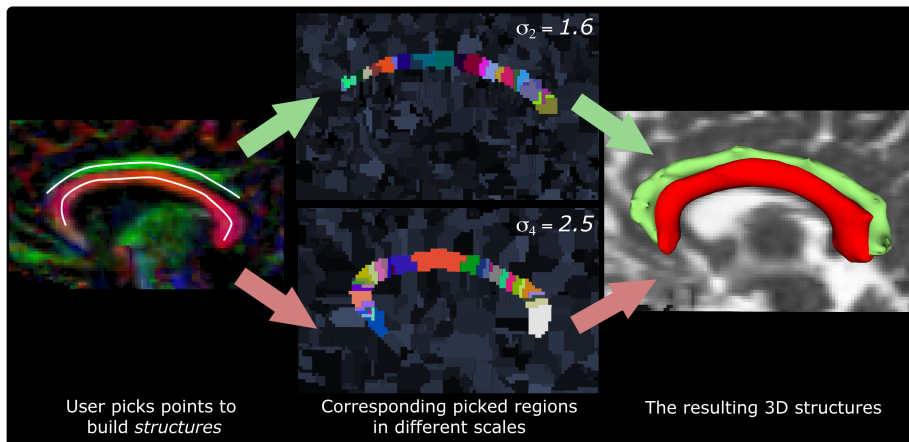


Fig. 7. A $128 \times 64 \times 64$ DTI brain image. The user selects points in his segmentation task (Left), the correspondent basins in the respective Selection Scale are highlighted (Middle) and a smooth isosurface wraps the grouped similar connected regions (Right).

5 Conclusions and Future Work

In this paper, we presented a hierarchical segmentation algorithm, using watersheds, for diffusion tensor fields. In a semi automatic manner, a hierarchical representation of the data is assembled providing a new way to visualize and interact with this type of data. A multitude of possibilities arise. The automatic partitioning of the data can be used to assess statistical properties of the data. Combined with other typical uses of DTI like fiber-tracking, this can be used to study the connectivity of the different regions of the brain. Although this work has a medical end goal, the framework is general.

The use of Log-Euclidean gradient embodies the watershed segmentation with a unclear intuition. It expresses dissimilarity between the diffusion tensors, however its connection to the underlying tissue structure is not clear. The use of other gradient alternatives, such as the tensorial morphological gradient [22] allowing the use of known distance measures [23], or Schultz's structure tensor [26] combining the intuitive Kindlmann's [27] decomposition of the tensor changes into six different gradients will be subject of future study.

Given the anisotropic nature of the brain tissue (as for muscle fibers), the use of a Gaussian isotropic kernel hinders the creation of an adequate scale space, preventing the hierarchical linking to give the desired results. However, the proposed tool is versatile enough to allow the semi-automatic segmentation of the structures of interest by combining the several building blocks. Future work will study the use of anisotropic kernels based on the diffusion tensor at each voxel as in [28] so to improve the inference of tissue archetype.

A more robust and anatomical significant improvement to the hierarchical linking lies on the use of homogeneity indices in addition to the spatial overlap between adjacent scales, since a bundle, by definition, groups together similar DTs.

The creation of a meaningful hierarchical representation of the data unravels new visualisation and interaction possibilities and thus novel ways to study diffusion tensor fields. One can use well-established techniques for graph visualization and interaction, to directly manipulate the data. Illustrative rendering may as well be used, to augment the more abstract graph visualization.

The proposed hierarchical methodology is also relevant for high angular resolution diffusion imaging (HARDI) given its close analytical connection to DTI.

Artificial and real data shows the potential of the presented method. However, doing a more elaborated evaluation is necessary, and a comparison to other methods should also be performed.

Acknowledgements

This work was supported by: Fundação para a Ciência e a Tecnologia (FCT, Portugal) under grant SFRH/BD/24467/2005, and the Netherlands Organization for Scientific Research (NWO-VENI grant 639.021.407). The authors would like to thank prof. dr. Luc Florack for the always insightful discussions on Scale Space.

References

1. Basser, P.J., Mattiello, J., Lebihan, D.: MR diffusion tensor spectroscopy and imaging. *Biophysical Journal* **66** (1994) 259–267
2. Vilanova, A., Zhang, S., Kindlmann, G., Laidlaw, D.: An introduction to visualization of diffusion tensor imaging and its applications. In Weickert, J., Hagen, H., eds.: *Visualization and Processing of Tensor Fields*. Mathematics and Visualization. Springer (2005) 121–153
3. Zhukov, L., Barr, A.H.: Heart-muscle fiber reconstruction from diffusion tensor MRI. In: *Proceedings of IEEE Visualization 2003*, IEEE Computer Society (2003) 597–602
4. Melhem, E.R., Mori, S., Mukundan, G., Kraut, M.A., Pomper, M.G., van Zijl, P.C.: Diffusion tensor MR imaging of the brain and white matter tractography. *American Journal of Roentgenology* **178**(1) (2002) 3–16
5. Wang, Z., Vemuri, B.C.: DTI segmentation using an information theoretic tensor dissimilarity measure. *IEEE Trans. Med. Imaging* **24**(10) (2005) 1267–1277

6. Zhukov, L., Museth, K., Breen, D., Whitaker, R., Barr, A.: Level set modeling and segmentation of DT-MRI brain data. *Journal of Electronic Imaging* **12**(1) (2003) 125–133
7. Rousson, M., Lenglet, C., Deriche, R.: Level set and region based surface propagation for diffusion tensor MRI segmentation. In Sonka, M., Kakadiaris, I.A., Kybic, J., eds.: *ECCV Workshops CVAMIA and MMBIA*. Volume 3117 of *Lecture Notes in Computer Science.*, Springer (2004) 123–134
8. Awate, S.P., 0005, H.Z., Gee, J.C.: A fuzzy, nonparametric segmentation framework for dti and mri analysis: With applications to dti-tract extraction. *IEEE Trans. Med. Imaging* **26**(11) (2007) 1525–1536
9. Moberts, B., Vilanova, A., van Wijk, J.J.: Evaluation of fiber clustering methods for diffusion tensor imaging. In: *IEEE Visualization, IEEE Computer Society* (2005) 9
10. Weldeselassie, Y., Hamarneh, G.: DT-MRI segmentation using graph cuts. In: *SPIE Medical Imaging*. (2007) 1–9
11. Florack, L.M.J., Astola, L.J.: A multi-resolution framework for diffusion tensor images. In Aja Fernández, S., de Luis Garcia, R., eds.: *CVPR Workshop on Tensors in Image Processing and Computer Vision*, Anchorage, Alaska, USA, June 24–26, 2008 1-7, IEEE (2008) *Digital proceedings*.
12. Meyer, F., Beucher, S.: Morphological segmentation. *Journal of Visual Communications and Image Representation* **1** (1990) 21–46
13. Niethammer, M., Zach, C., Melonakos, J., Tannenbaum, A.: Near-tubular fiber bundle segmentation for diffusion weighted imaging: segmentation through frame reorientation. (03 2009)
14. Sporring, J.: *Gaussian Scale-Space Theory*. Kluwer Academic Publishers, Norwell, MA, USA (1997)
15. Florack, L., Kuijper, A.: The topological structure of scale-space images. *J. Math. Imaging Vis.* **12**(1) (2000) 65–79
16. Dam, E., Nielsen, M.: Non-linear diffusion for interactive multi-scale watershed segmentation. In: *MICCAI '00: Proceedings of the Third International Conference on Medical Image Computing and Computer-Assisted Intervention*, London, UK, Springer-Verlag (2000) 216–225
17. Arsigny, V., Fillard, P., Pennec, X., Ayache, N.: Log-Euclidean metrics for fast and simple calculus on diffusion tensors. *Magnetic Resonance in Medicine* **56**(2) (August 2006) 411–421
18. Fillard, P., Arsigny, V., Pennec, X., Ayache, N.: Clinical DT-MRI estimation, smoothing and fiber tracking with log-Euclidean metrics. *IEEE Trans. Med. Imaging* **26**(11) (November 2007) 1472–1482 PMID: 18041263.
19. Pennec, X., Fillard, P., Ayache, N.: A Riemannian framework for tensor computing. *Int. J. Comput. Vision* **66**(1) (January 2006) 41–66 A preliminary version appeared as INRIA Research Report 5255, July 2004.
20. Kindlmann, G.: Superquadric tensor glyphs. In: *Proceeding of The Joint Eurographics - IEEE TCVG Symposium on Visualization*. (May 2004) 147–154
21. Maxwell, J.C.: On hills and dales. Volume XL. *The London, Edinburgh and Dublin Philosophical Magazine and Journal of Science* (1870)
22. Rittner, L., Lotufo, R.A.: Diffusion tensor imaging segmentation by watershed transform on tensorial morphological gradient. In: *Proceedings, Los Alamitos, IEEE Computer Society* (Oct. 12–15, 2008 2008)
23. Peeters, T., Rodrigues, P., Vilanova, A., ter Haar Romeny, B.: Analysis of distance/similarity measures for diffusion tensor imaging. In Laidlaw, D.H., Weickert,

- J., eds.: Visualization and Processing of Tensor Fields: Advances and Perspectives. Springer, Berlin (2008) in Press.
24. Stejskal, E.O., Tanner, J.E.: Spin diffusion measurements: Spin echoes in the presence of a time-dependent field gradient. *The Journal of Chemical Physics* **42**(1) (1965) 288–292
 25. Alexander, D.C., Barker, G.J., Arridge, S.R.: Detection and modeling of non-gaussian apparent diffusion coefficient profiles in human brain data. *Magnetic Resonance in Medicine* **48**(2) (2002) 331–340
 26. Schultz, T., Burgeth, B., Weickert, J.: Flexible segmentation and smoothing of DT-MRI fields through a customizable structure tensor. In: *Advances in Visual Computing. Lecture Notes in Computer Science*, Springer (2006) 455–464
 27. Kindlmann, G.L., Estépar, R.S.J., Niethammer, M., Haker, S., Westin, C.F.: Geodesic-loxodromes for diffusion tensor interpolation and difference measurement. In Ayache, N., Ourselin, S., Maeder, A.J., eds.: *MICCAI* (1). Volume 4791 of *Lecture Notes in Computer Science.*, Springer (2007) 1–9
 28. Chung, M.K., Chung, M.K., Lazar, M., Lazar, M., Alexander, A.L., Alexander, A.L., Lu, Y., Lu, Y., Davidson, R., Davidson, R.: Probabilistic connectivity measure in diffusion tensor imaging via anisotropic kernel smoothing. Technical Report 1081, UW Dept. of Stat. (2003)